Phytochemistry 117 (2015) 98–106

Contents lists available at ScienceDirect

Phytochemistry

journal homepage: www.elsevier.com/locate/phytochem

Flavonoids from *Piper delineatum* modulate quorum-sensing-regulated phenotypes in *Vibrio harveyi*

Alberto J. Martín-Rodríguez [a,b], Juan C. Ticona [c], Ignacio A. Jiménez [a], Ninoska Flores [c], José J. Fernández [a,*], Isabel L. Bazzocchi [a,*]

[a] Instituto Universitario de Bio-Orgánica Antonio González and Departamento de Química Orgánica, Universidad de La Laguna, Avenida Astrofísico Francisco Sánchez 2, 38206 La Laguna, Tenerife, Spain
[b] Plataforma Oceánica de Canarias (PLOCAN), Carretera de Taliarte s/n, 35214 Telde, Gran Canaria, Spain
[c] Instituto de Investigaciones Fármaco Bioquímicas, Facultad de Ciencias Farmacéuticas y Bioquímicas, Universidad Mayor de San Andrés, Avenida. Saavedra 2224, Miraflores, La Paz, Bolivia

ARTICLE INFO

Article history:
Received 18 January 2015
Received in revised form 28 May 2015
Accepted 2 June 2015
Available online 10 June 2015

Keywords:
Piper delineatum
Flavonoids
Quorum sensing
Biofilm
Vibrio harveyi

ABSTRACT

Quorum sensing (QS), or bacterial cell-to-cell communication, is a key process for bacterial colonization of substrata through biofilm formation, infections, and production of virulence factors. In an ongoing investigation of bioactive secondary metabolites from *Piper species*, four new flavonoids (**1**–**4**), along with five known ones (**5**–**9**) were isolated from the leaves of *Piper delineatum*. Their stereostructures were established by spectroscopic and spectrometric methods, including 1D and 2D NMR experiments, and comparison with data reported in the literature. The compounds were screened for their ability to interfere with QS signaling in the bacterial model *Vibrio harveyi*. Four compounds from this series (**2**, **3**, **6**, and **7**) exhibited remarkable activity in the micromolar range, being compounds **3** and **7** particularly attractive since they did not affect bacterial growth. The results suggest that these flavonoids disrupt QS-mediated bioluminescence by interaction with elements downstream LuxO in the QS circuit of *V. harveyi*, and also, they exhibited a strong dose-dependent inhibition of biofilm formation. The present findings shed light on the QS inhibition mechanisms of flavonoids, underlining their potential applications.

1. Introduction

One of the most ground-breaking developments of microbiological research during the past 40 years has been the recognition of bacterial biofilms as the predominant bacterial lifestyle (Mielich-Suss and López, 2015). Biofilms play an important role in the fouling process (Yebra et al., 2004), and they are also postulated as being responsible for an overwhelming proportion of persistent antibiotic resistance (Bjarnsholt et al., 2013), one of the major obstacles in antimicrobial chemotherapy.

Quorum sensing (QS) is the term coined for bacterial cell-to-cell communication, a process that regulates coordinated behaviors in bacteria as a function of population density. It involves the production, excretion and detection of autoinducer (AI) molecules that trigger the expression of QS-regulated genes (Miller and Bassler, 2001). This process allows bacteria to optimize their energetic resources to carry out tasks that are more efficiently performed when a threshold population is achieved, for example, the production of virulence factors, biofilm formation and, in certain bacteria such as *Vibrio harveyi*, the generation of bioluminescence (Waters and Bassler, 2005). Since quorum sensing inhibitors (QSIs) do not target bacterial growth, they do not exert a selective pressure on bacterial populations and, consequently, they avoid the appearance of resistance towards chemical or antibiotic treatments (Kalia, 2013), although their prospects are still being debated (Defoirdt et al., 2010; García-Contreras et al., 2013). Furthermore, there is increasing evidence that QS signaling molecules interact directly with fouling colonizers (Joint et al., 2007), and conversely, QS disruption controls, directly or indirectly, biofilm formation and larval attachment onto underwater substrata (Dobretsov et al., 2007; Twigg et al., 2014). Renowned examples are the brominated furanones produced by the red alga *Delisea pulchra* (Givskov et al., 1996). Therefore, the search for effective and safe QSIs has become a priority for current antifouling research as well as for biomedicine, industry and other fields where bacterial biofilms are causes of sanitary or operational problems. In this context, flavonoids, which are among the richest members of plant-derived compounds in terms of structural diversity and biological activity (Andersen and Markham, 2006), have been reported

* Corresponding authors.
E-mail addresses: jjfercas@ull.es (J.J. Fernández), ilopez@ull.es (I.L. Bazzocchi).

http://dx.doi.org/10.1016/j.phytochem.2015.06.006
0031-9422/

as potential inhibitors of both biofilm formation and virulence factors in pathogenic bacteria by interfering with QS mechanisms (Cushnie and Lamb, 2011; Nazzaro et al., 2013).

The goal of this work is: (a) to report the isolation and structural elucidation of flavonoids from *Piper delineatum*, (b) to report the results from their screening as disruptors of QS-regulated phenotypes using *V. harveyi* as bacterial model, (c) to select the most active compounds and gain an insight into their possible mode of action through phenotypic analyses with three *V. harveyi* mutant strains, and (d) to check whether these compounds were also able to interfere with bacterial adhesion to material substrates (biofilm formation).

Thus, efforts have been focused on the characterization of new flavonoids as potential QSIs from *P. delineatum* Trel. (Piperaceae), a shrub native to tropical regions of the Americas, and whose chemical investigation has not been previously reported. In this work, the isolation, structure elucidation and bioactivity of nine flavonoids, including two new chalcones and two new flavanones (**1**–**4**) from the leaves of *P. delineatum*, are reported. Their sterostructures were elucidated by means of ^{1}H and ^{13}C NMR spectroscopic studies, including homonuclear (COSY and ROESY) and heteronuclear (HSQC and HMBC) correlation experiments. These flavonoids are able to interfere with bacterial QS-controlled processes using *V. harveyi* as bacterial model.

V. harveyi is a marine luminescent bacterium with a complex QS system (Henke and Bassler, 2004) (Fig. 1). *V. harveyi* employs three kinds of autoinducers for intra-species (HAI-1 signal, a homoserine lactone), intra-genera (CAI-1 signal, an α-amino ketone) and inter-species (AI-2 signal, a furanosyl borate diester) communication in three parallel circuits that converge in the σ^{54}-dependent response regulator LuxO, which is phosphorylated (low cell densities, or more precisely, low AI concentrations) or dephosphorylated (high AI concentrations) via the phosphotransferase protein LuxU. At low AI concentrations, the phosphorylated LuxO activates the translation of five small quorum-regulatory RNAs (Qrr sRNAs) that, together with the chaperone Hfq destabilize the mRNA encoding the QS master regulator LuxR. Once a threshold concentration of AIs is achieved, the QS receptors LuxN, LuxPQ and CqsS switch from kinases to phosphatases, dephosphorylating LuxO, thus allowing the expression of LuxR and the subsequent translation of the genes in the QS regulon (Pompeani et al., 2008; Anetzberger et al., 2012; Nackerdien et al., 2008).

In order to characterize the bioactivities of the isolated flavonoids and gain an insight into their molecular targets, four compounds exhibiting a promising profile (**2**, **3**, **6** and **7**) were evaluated with *V. harveyi* QS mutants. Whereas compounds **2** and **6** exerted an activity with toxic side effects, compounds **3** and **7** disrupted QS-regulated bioluminescence in a non-toxic fashion, probably by interaction with elements downstream LuxO in the QS transduction pathway. These flavonoids also imposed strong, dose-dependently inhibitions on biofilm formation, a process controlled by QS in *V. harveyi*.

2. Results and discussion

2.1. Isolation and structure identification

The EtOH extract of leaves of *P. delineatum* were partitioned into a CH_2Cl_2/H_2O (1:1, v/v) solution. The CH_2Cl_2 fraction was subjected to multiple chromatographic steps, involving vacuum-liquid and medium-pressure liquid chromatography, centrifugal preparative TLC, and preparative TLC chromatography on Si gel, and Sephadex LH-20 to yield flavonoids **1**–**9** (Fig. 2). The structures of the new compounds were deduced as described below.

Compound **1** was obtained as a yellow amorphous solid and showed the molecular formula $C_{18}H_{18}O_6$ by HREIMS analysis (*m/z* 330.1104, calcd 330.1103). The IR absorption bands at 3375, 1725, 1628 and 726 cm^{-1} indicated hydroxyl, carbonyl and aromatic functions, and the UV absorption maximum at 345 nm was consistent with **1** being a chalcone derivative (Fu et al., 1993). The ^{13}C NMR spectrum [$(CD)_3CO$] showed peaks corresponding to 18 carbons (Table 1), which were classified into three CH_3, seven

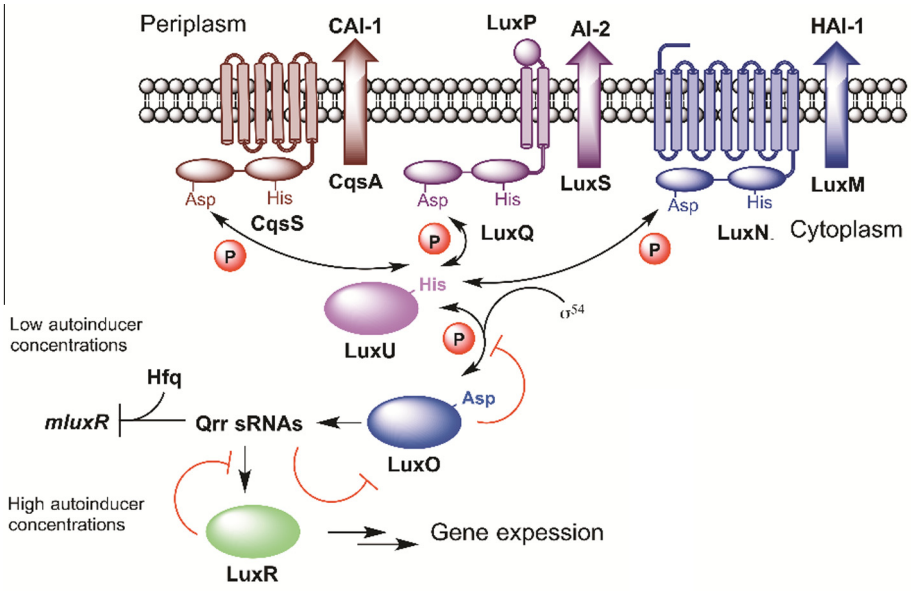

Fig. 1. The QS signaling pathway of *Vibrio harveyi*. Three AIs, HAI-1, CAI-1 and AI-2 are believed to mediate intra-species, intra-genus and inter-species communication, respectively. These AIs are produced by the synthases LuxM, LuxS and CqsA, respectively, and excreted to the extracellular milieu. At low AI concentrations, the two-component systems LuxN, LuxPQ and CqsS transfer phosphate to the phosphotransferase protein LuxU, which in turn phosphorylates the σ^{54}-dependent response regulator LuxO. When phosphorylated, LuxO and the chaperone Hfq activate the translation of five Qrr sRNAs that destabilize the messenger RNA encoding the QS master regulator LuxR (mluxR). By contrast, at high AI concentrations, LuxN, LuxPQ and CqsS switch from kinases to phosphatases, depriving LuxO of phosphate and allowing the expression of LuxR and the QS-regulated genes, including those encoding luciferase biosynthesis.

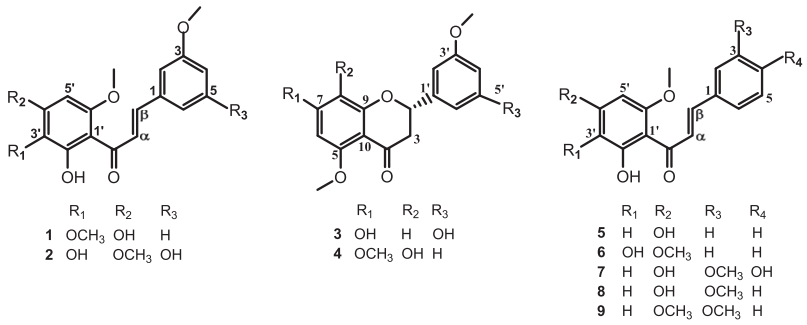

Fig. 2. Chemical structure of the flavonoids **1**–**9** from *P. delineatum*.

Table 1
NMR spectroscopic data[a] (δ, J in Hz in parentheses) for compounds **1**–**4**.

Position	**1**		**2**		**3**		**4**	
	δ_H	δ_C, mult.	δ_H	δ_C, mult.	δ_H	δ_C, mult.	δ_H	δ_C, mult.
1		137.8, C		138.3, C				
2	7.27 d (2.4)	114.2, CH	6.82 s	108.4, CH	5.35 dd (3.1, 12.4)	79.6, CH	5.48 dd (3.0, 12.3)	80.0, CH
3		161.1, C		159.8, C	2.63 dd (3.1, 16.3)	46.4, CH_2	2.70 dd (3.0, 16.4)	46.7, CH_2
					2.88 dd (12.4, 16.3)		2.97 dd (12.3, 16.4)	
4	7.01 dd (2.4, 8.0)	117.0, CH	6.50 t (2.0)	104.4, CH				
5	7.37 t (8.0)	130.9, CH		162.3, C		163.7, C		155.3, C
6	7.31 d (8.0)	121.7, CH	6.78 s	106.3, CH	6.14 d (2.1)	94.1, CH	6.40 s	91.8, CH
7						165.2, C		154.1, C
8					6.09 d (2.1)	96.7, CH		129.6, C
9						165.5, C		151.0, C
10						106.0, C		107.0, C
C=O		193.7, C		194.1, C		187.9, C		188.4, C
α	7.99 d (15.5)	128.8, CH	7.95 d (15.6)	128.6, CH				
β	7.73 d (15.5)	142.9, CH	7.65 d (15.6)	143.3, CH				
1′		106.6, CH		107.1, C		142.9, C		142.1, C
2′		160.8, C		154.0, C	6.59 br s	104.1, CH	7.16 s	113.0, CH
3′		130.0, C		129.2, C		159.7, C		160.9, C
4′		158.1, C		154.3, C	6.40 t (2.2)	101.9, CH	6.93 dd (2.4, 8.0)	114.5, CH
5′	6.13 s	91.7, CH	6.35 s	89.2, CH		162.1, C	7.33 t (8.0)	130.4, CH
6′		159.8, C		156.6, C	6.60 br s	106.6, CH	7.11 d (8.0)	119.3, CH

[a] Spectra recorded in $(CD_3)_2CO$ at 400 (^1H) and 100 (^{13}C) MHz. Data are based on DEPT, HSQC, and HMBC experiments.

sp^2 CH, seven sp^2 quaternary carbons, and one keto-carbonyl carbon by analysis of DEPT experiments. The ^1H NMR spectrum displayed 18 proton signals (Table 1), suggesting the presence of two hydroxy groups in the molecule. The direct connectivity of the proton and carbon atoms was determined by a HSQC experiment. The presence of a *trans-o*-coumaroyl [(2*E*)-3-(3-methoxyphenyl)-2-propenoyl] moiety was suggested to be *meta*-substituted on the basis of the coupling patterns of the aromatic protons in the ^1H NMR spectrum and COSY experiment, which showed four aromatic proton resonances at δ 7.01 (1H, dd, J = 2.4, 8.0 Hz; H-4), 7.27 (1H, d, J = 2.4 Hz; H-2), 7.31 (1H, d, J = 8.0 Hz; H-6), and 7.37 (1H, t, J = 8.0 Hz; H-5). The ^1H-^1H COSY correlations between H-2/H-4, H-4/H-5, H-5/H-6, and H-α and H-β confirmed the connectivity deduced from coupling constants analysis. The fragment ion at m/z 196 ($[M]^+$ – $C_9H_8O_5$), formed from the bond cleavage at C=O—Cα in the EIMS, supported the presence of this moiety. The large coupling constant (J = 15.5 Hz) between H-α and H-β signals suggested an *E*-geometry of the Cα–Cβ double bond. In similar fashion, the structure of the ring A was identified as a penta-substituted aromatic ring with four oxygen substituents, the side chain of C_3, and a single proton at δ_H 6.13. In its ^1H NMR spectrum, signals assignable to three methoxy groups at δ_H 3.77, 3.87, and 3.97 were also observed. These spectroscopic data are consistent with a chalcone skeleton with two hydroxy and three methoxy groups distributed on penta-substituted and di-substituted aromatic rings. The structure proposed was corroborated by analysis of 2D NMR data, including HSQC, HMBC and ROESY experiments. The region-substitution of **1** was determined by an HMBC experiment showing couplings between the singlet aromatic proton at δ_H 6.13 (H-5′) to C-1′ (δ_C 106.6), C-3′ (δ_C 130.0), C-4′ (δ_C 158.1), and C-6′ (δ_C 159.8); cross-peak between the singlet phenolic proton at δ_H 14.34 (OH-2′) to C-1′ (δ_C 106.6), C-3′ (δ_C 130.0), and C-2′ (δ_C 160.8); correlation of the signal at δ_H 3.77 (OCH_3-3′) with C-3′ (δ_C 130.0), and that at δ_H 3.97 (OCH_3-6′) with C-6′ (δ_C 159.8), confirming the positions for the hydroxy and methoxy groups on the A ring. In similar fashion, the substitution pattern of the B ring was supported by correlations of the aromatic proton at δ_H 7.27 (H-2) with C-1 (δ_C 137.8), C-3 (δ_C 161.1), C-4 (δ_C 117.0), and C-β (δ_C 142.9). The space correlations by 2D NMR experiment further confirmed the structure of **1**, showing NOEs of the methoxy protons OCH_3-3 (δ_H 3.87) to H-2 (δ_H 7.27) and H-4 (δ_H 7.01), and those from OCH_3-6′ (δ_H 3.97) to H-5′ (δ_H 6.13). This evidence, and comparison with reported data for related compounds (Aponte et al., 2010), allowed us to establish the structure of compound **1** as 2′,4′-dihydroxy-3,3′,6′-trimethoxychalcone.

The HREIMS of **2** furnished a $[M]^+$ at m/z 346.1053, consistent with a molecular formula of $C_{18}H_{18}O_7$. The ^1H NMR spectrum (Table 1) displayed 18 proton signals, including typical chemical shifts and coupling pattern of CH=CH protons of the *trans* system of chalcones with one chelated hydroxyl proton signal at δ_H 13.81 (1H, s, HO-2′), two phenolic proton signals at δ_H 8.62 (1H, br, HO-3) and δ_H 6.91 (1H, s, HO-3′), and three methoxy groups at δ_H 3.82

(3H, s, CH_3O-5), 3.96 (3H, s, CH_3O-4′) and 4.01 (3H, s, CH_3O-6′). These data were supported by the ^{13}C NMR spectrum [$(CD_3)_2CO$] (Table 1) displaying 18 carbon resonances, in agreement with the molecular formula. Compound **2** was closely related to **1**, and consequently, its structure elucidation was greatly aided by comparison of their spectroscopic data. Its NMR spectra revealed the presence of an additional phenol group and the concomitant absence of the proton signal. Even so, a complete set of 2D NMR spectra (COSY, ROESY, HSQC and HMBC) was acquired for **2** in order to gain the complete and unambiguous assignment of the ^1H and ^{13}C NMR chemical shifts and region-substitution patterns. Thus, the molecular structure of compound **2** was deduced as 2′,3′,5-trihydroxy-4′,6′,3-trimethoxychalcone.

Compound **3** was obtained as a yellow amorphous solid, and its HREIMS spectrum showed a molecular ion peak at *m/z* 316.0932 (calcd 316.0947), indicating the molecular formula $C_{17}H_{16}O_6$, which was supported by ^{13}C and DEPT NMR analysis. The IR absorption bands at 3432, 1729, 1605 and 756 cm^{-1} indicated hydroxyl, carbonyl and aromatic functions, and the UV spectrum showing an absorption band at 284 nm suggested the presence of a flavanone skeleton (Harborne and Mabry, 1975). The ^{13}C NMR spectrum [$(CD_3)_2CO$] (Table 1) showed peaks corresponding to 17 carbons, which were classified into two CH_3, one sp^3 CH_2, one sp^3 CH, five sp^2 CH, seven sp^2 quaternary carbons, and one keto-carbonyl carbon by analysis of DEPT experiments. The ^1H NMR spectrum (Table 1) displayed 16 proton signals, including singlet signals at δ 9.41 and 8.51, characteristic for downfield exchangeable phenolic protons, and signals assignable to two methoxy groups at δ 3.77 and 3.79. The presence of a flavanone structure was evidenced by an ABX spin system, including resonances at δ_H 5.35 (dd, J_{AX} = 3.1, J_{BX} = 12.4 Hz, H-2), δ_H 2.88 (dd, J_{BX} = 12.4 Hz, J_{AB} = 16.3 Hz, H-3_{ax}) and δ_H 2.63 (dd, J_{AX} = 3.1 Hz, J_{AB} = 16.3 Hz, H-3_{eq}). An AB pattern with signals at δ_H 6.14 (d, J_{AB} = 2.1 Hz, H-6) and δ_H 6.09 (d, J_{AB} = 2.1 Hz, H-8), and an ABC pattern with signals at δ_H 6.60 (br s, H-6′), 6.59 (br s, H-2′) and 6.40 (t, J = 2.2 Hz, H-4′), whose multiplicity and small coupling constants were indicative of a tetra-substituted A-ring and a 2,4,6-substituted B-ring, were also observed in the ^1H and COSY NMR spectra. The structure proposed was corroborated by analysis of 2D NMR data, including HSQC, HMBC and ROESY experiments. The methoxy groups were established to be attached at C-5′ and C-5 on the basis of ^1H–^{13}C long-range correlations from proton signals at δ_H 3.77 and 3.79 to carbon signals at δ_C 162.1 and 163.7, respectively. The ROESY experiment showing NOEs from H-4′ and H-6′ to MeO-5′ (δ 3.77) as well as correlation between H-6 and MeO-5 (δ 3.79) was consist with the proposed structure. The configuration at C-2 was suggested as *S* by the levorotatory optical rotation (−11.1°), and the *trans* diaxial $J_{2,3}$ of 12.4 Hz (Tan et al., 2007). Consequently, the structure of **3** was assigned as (−)-2*S*-7,5′-dihydroxy-5,3′-dimethoxyflavonone.

Compound **4** was closely related to **3** and its HREIMS showed a molecular ion at *m/z* 330.1111 ($C_{18}H_{18}O_6$), 14 mass units higher than that of **3**, indicating the presence of an additional methoxy group compared to **3**. The ^1H NMR spectrum of **4** (Table 1) showed chemical shifts and coupling pattern of a pyranone moiety, CH–CH_2, characteristic in flavanones, and the coupling pattern of protons H-2′, H-4′, H-5′ and H-6′ indicated a *meta*-substituted aryl at C-2. Only one aromatic proton with a rather high field chemical shift at δ_H 6.40 (s) was left on the A ring. The 1D NMR spectroscopic data of **4** were similar to those of **3** with the main differences being the region-substitution pattern on A and B rings. 2D NMR experiments allowed the complete and unambiguous assignment of the ^1H and ^{13}C NMR chemical shifts (Table 1), region-substitution, and relative configuration of compound **4**. The absolute configuration at C-2 was proposed as *S* based on the negative optical rotation value (−12.1°) and biogenetic means (Andersen and Markham, 2006). Thus, the structure for **4** was deduced as (−)-2*S*-8-hydroxy-5,7,3′-trimethoxyflavonone.

The known compounds **5**–**9** were identified as 2′,4′-dihydroxy-6′-methoxychalchone (**5**) (Kuroyanagi et al., 1983), 2′,3′-dihydroxy-4′,6′-dimethoxychalchone (**6**) (Chantrapromma et al., 2000), 2′,4′,4-trihydroxy-3,6′-dimethoxychalchone (**7**) (Vogel et al., 2010), 2′,4′-dihydroxy-3,6′-dimethoxychalchone (**8**) (Aponte et al., 2010) and 2′-hydroxy-3,4′,6′-trimethoxychalchone (**9**) (Boumendjel et al., 2008) by comparison of their spectroscopic data with values reported in the literature.

2.2. Quorum sensing inhibition assays

To assess the potential QS inhibitory activity of the isolated compounds, two screening rounds were conducted using the *V. harveyi* reporter strains BB886 (*luxPQ*::Tn5Kan, unable to detect AI-2) and BB170 (*luxN*::Tn5Kan, unable to detect HAI-1). In the first-round screening the test compounds were evaluated at the cut-off dose of 100 μM (Fig. 3). Due to their inhibitory activity in both signaling pathways, three chalcones (**2**, **6** and **7**) and one flavanone (**3**) were selected from this initial assay to perform a second-round screening with the reporter strains BB886 and BB170. Twofold serial dilutions of the compounds, from 500 to 15.6 μM, were assayed. Luminescence was monitored every 15 min over 18 h. In parallel, OD_{600} was measured in order to correlate simultaneously the inhibition caused in bacterial bioluminescence with any possible toxic effect. This is important to remark since bioluminescence strongly depends on the physiological state of the cells, the population density and the growth rate. Thus, endpoints based on discrete measurements may conduct to misleading results, as recently reviewed (Defoirdt et al., 2013). At concentrations up to 1.25% (v/v), which is the highest amount of solvent, DMSO did not have a significant effect either on bacterial luminescence or on bacterial growth ($p > 0.05$, Dunnett's test). The decrease caused in the luminescence of both HAI-1^- and AI-2^- mutants by the *trans*-chalcones **2** and **6** was dose-dependent, but associated with toxicity (Figs. 4A, C and 5A, C). Accordingly, the IC_{50} values for HAI-1 and AI-2 inhibition were close to those obtained for growth inhibition (Table 2). A different behavior is deduced from the luminescence and growth data in the presence of flavonoids **3** and **7** (Figs. 3B, D and 4B, D). For these compounds, the IC_{50} values obtained for the HAI-1 signaling pathway were lower than their counterparts in the AI-2 pathway (Table 2). However, according to the behavior displayed by both compounds towards *V. harveyi* strains with non-functional LuxN and LuxPQ receptors, a lack of specific antagonism towards one receptor or the other can be inferred. In this regard, it should be noted that even though the average IC_{50} value for compound **7** in the HAI-1^- mutant was above 500 μM (Table 2), values very close to 50% inhibition were recorded at the highest test dose of 500 μM (Fig. 4D). Furthermore, these two flavonoids exerted a negligible effect on bacterial growth, thus highlighting their non-toxic mode of action (Fig. 5B and D). It is important to recall that the IC_{50} values reported herein have been obtained under high-density conditions (starting cell density of around 10^7 cfu ml^{-1}) and have been calculated taking into account their cumulative effect over an 18 h period instead of a short-term effect at the initial stages of the culture. These are the most restrictive conditions and explain the relatively high effective doses of these compounds.

To confirm that these flavonoids target downstream elements in the QS transduction pathway, compounds **3** and **7** were selected for further evaluation due to their lack of toxicity, which makes them attractive candidates for potential applications. Therefore, both flavonoids were assayed against the reporter strain *V. harveyi* BB721, a constitutively bright mutant in which the phosphorelay activity of LuxO has been lost after transposon insertion

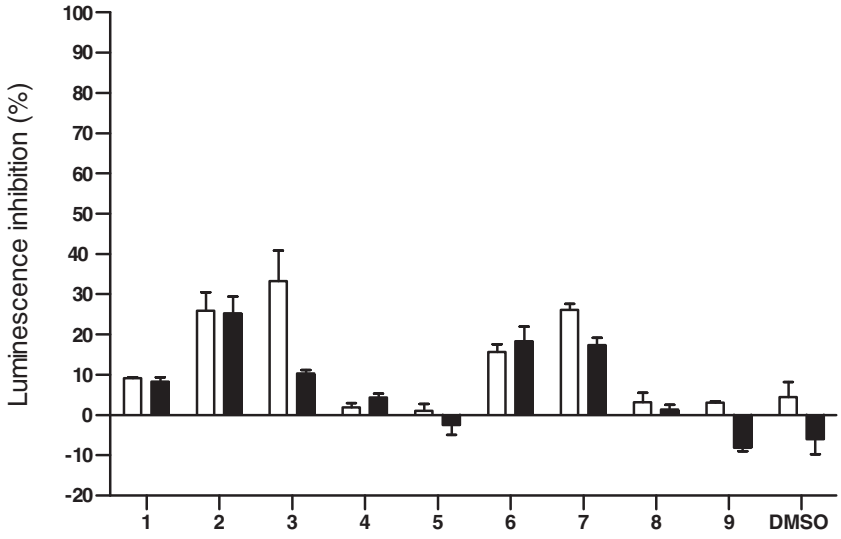

Fig. 3. Inhibition of bioluminescence displayed by the flavonoids screened in this study at the cut-off concentration of 100 μM in the *V. harveyi* mutants BB886 (white bars, lacks the AI-2 sensor) and BB170 (black bars, lacks the HAI-1 sensor). Bars represent the mean ± SD of three replicates. The % inhibition is referred to an untreated control. Data represent the integrated luminescence values at each dose over an 18 h period of constant monitoring.

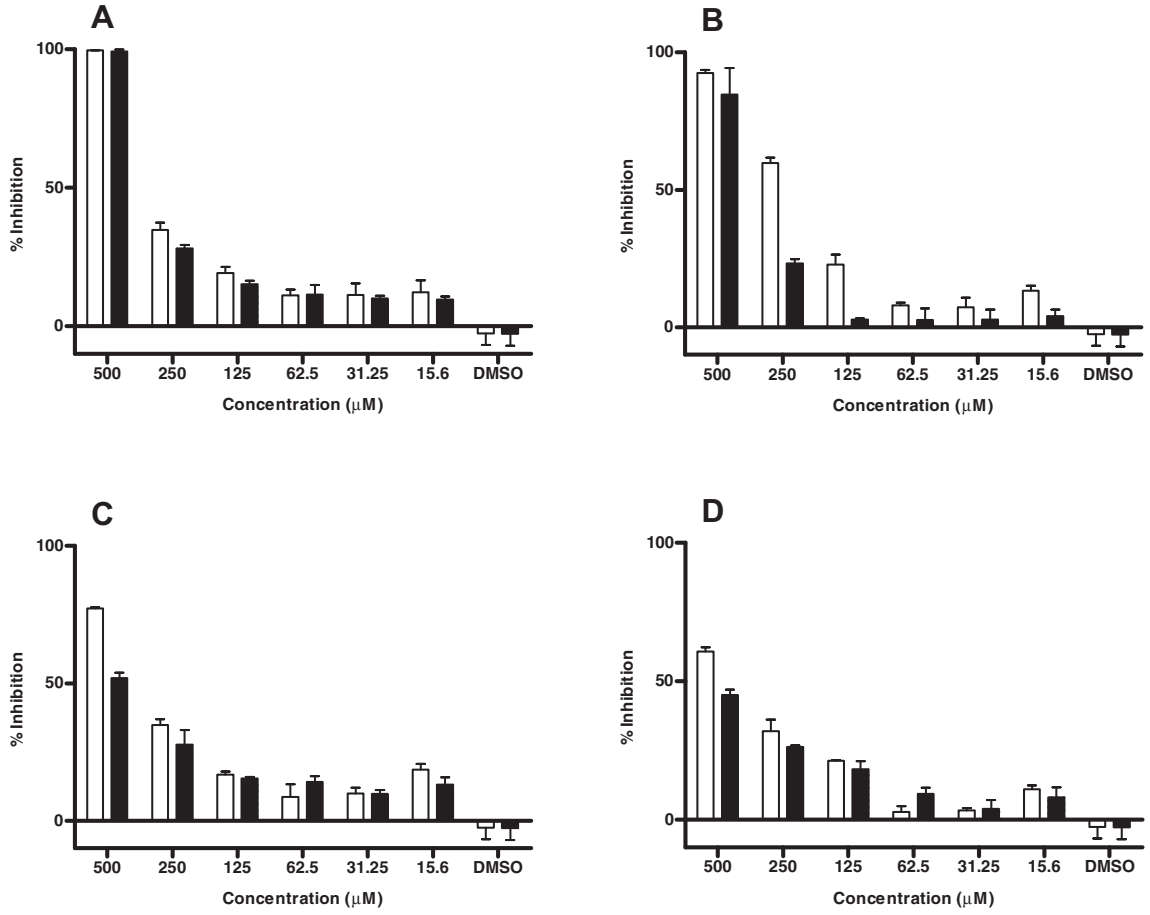

Fig. 4. Normalized luminescence inhibitions (relative to untreated control) for *V. harveyi* BB886 (white bars) and BB170 (black bars) in the presence of compounds **2** (A), **3** (B), **6** (C) and **7** (D) at different doses from 500 to 15.6 μM. Bars represent the mean ± SD of three replicates. Data represent the integrated luminescence values at each dose over an 18 h period of constant monitoring.

(*luxO*::Tn5lacZ). Thus, this strain produces maximum luminescence per cell, regardless of the concentration of AIs. For this experiment a single concentration was tested (250 μM). Both flavonoids **3** and **7** inhibited bioluminescence very significantly (62% and 45%, respectively) with respect to the untreated control (Fig. 6). This result, together with the lack of toxicity of these compounds,

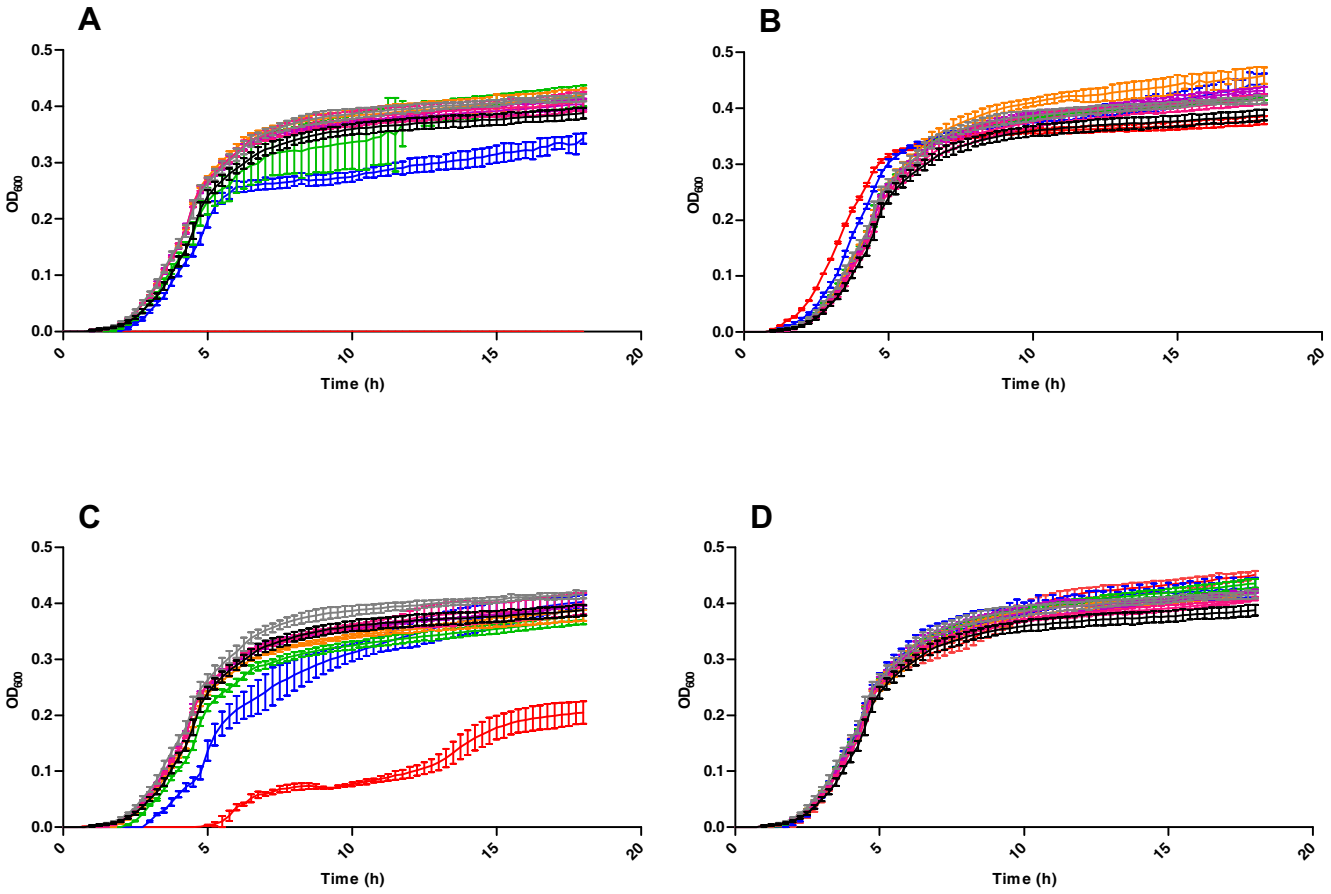

Fig. 5. Growth curves for *V. harveyi* BB120 (wild type strain) in the presence of compounds **2** (A), **3** (B), **6** (C) and **7** (D) at different test concentrations (red = 500 μM; blue = 250 μM; green = 125 μM; orange = 62.5 μM; purple = 31.25 μM; magenta = 15.6 μM; gray = 1.25% DMSO; black = untreated control). Data represent the mean ± SD of three replicates. (For interpretation of the references to colour in this figure legend, the reader is referred to the web version of this article.)

Table 2
Half-maximal inhibitory concentrations (IC_{50}) caused by compounds **2**, **3**, **6** and **7** on HAI-1 and AI-2-mediated bioluminescence and bacterial growth. Values (μM) represent the average of three replicates.

Compound	HAI-1 inhibition	AI-2 inhibition	Growth inhibition
2	278	291	290
3	206	349	>500
6	304	>500	388
7	385	>500	>500
Pentyl triphenylphosphonium bromide[a]	179	129	>500

[a] Reference substance used as internal control according to published data (Martín-Rodríguez et al., 2015).

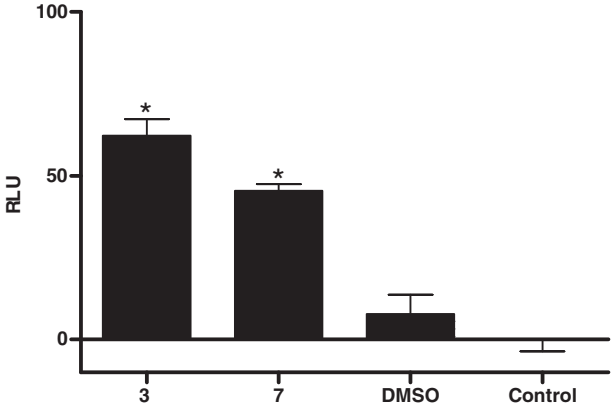

Fig. 6. Bioluminescence of *V. harveyi* BB721 (LuxO null) in the presence of compounds **3** and **7** at 250 μM, the proportional amount of solvent (DMSO, 0.6% v/v), and in the absence of treatment (control). Bars represent the mean ± SD of three replicates. Asterisks indicate significant differences with respect to the control ($p < 0.001$, Dunnett's test).

suggests that modulation of bioluminescence production in *V. harveyi* may be due to the interaction with elements downstream LuxO in the QS signal transduction circuit. It remains to be determined whether the compounds act at the transcriptional, posttranscriptional or enzymatic level.

The inhibitory effect of plant secondary metabolites, particularly flavonoids, on bacterial processes has been the focus of intensive research over the last few years (Kalia, 2013; Cushnie and Lamb, 2011). Recently, catechin has been reported as a QS disruptor, being able of inhibiting violacein production in *Chromobacterium violaceum* CVO26, as well as biofilm formation and elastase production in *Pseudomonas aeruginosa* PAO1 through interference with AI reception (Vandeputte et al., 2010). In a similar study (Vandeputte et al., 2011), the QS inhibitory properties of naringenin in *C. violaceum* CVO26 and in *P. aeruginosa* PAO1 pointed to a disruption in both AI production and in the C4-HSL-RlhR complex. Flavonoids have also demonstrated their ability to thwart cell-to-cell communication in *V. harveyi*. Vikram and co-workers reported the interference with both HAI-1 and AI-2 signaling pathways in *V. harveyi* by a series of commercial flavonoids (Vikram et al., 2010). In that study, the authors

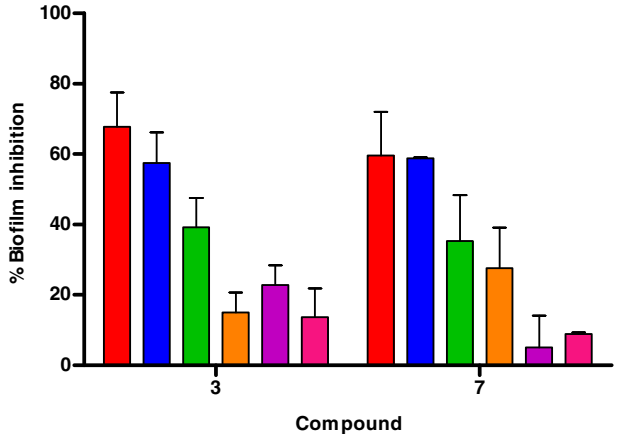

Fig. 7. Inhibition of biofilm formation caused by compounds **3** and **7** on *V. harveyi* BB120 at different concentrations (red = 500 μM; blue = 250 μM; green = 125 μM; orange = 62.5 μM; purple = 31.25 μM; magenta = 15.6 μM). Bars represent the mean ± SD of three replicates. (For interpretation of the references to color in this figure legend, the reader is referred to the web version of this article.)

suggested a possible target at LuxU or downstream this element for flavonoids such as naringenin that did not display any preferential response towards the HAI-1$^-$ or the AI-2$^-$ biosensor, which is in good agreement with our findings.

Since biofilm formation is also a QS-regulated process in *V. harveyi* (Waters and Bassler, 2006), we investigated the effect of compounds **3** and **7** on biofilm production. Indeed, a clear dose-dependent reduction of biofilm formation was observed in *V. harveyi* wild type strain in the presence of both compounds, with inhibitions as high as 68% and 60% for compounds **3** and **7**, respectively (Fig. 7). This result is in fair agreement with the effect observed in the QS-mediated bioluminescence at the same range of concentrations. Thus, taking these results together, it is deduced that suppression of biofilm formation likely occurs through disruption of cell-to-cell communication, without affecting bacterial growth. Given that *V. harveyi* is a causative agent of vibriosis in shrimp aquaculture (Rutherford and Bassler, 2012) and its QS system shares a high similarity with that of the human pathogen *Vibrio cholerae* (lacking the HAI-1/LuxM/LuxN system) (Defoirdt et al., 2008), the present findings constitute a promising starting point for the design of effective alternatives or complements to antibiotic treatments. Moreover, to investigate the impact on luminescence in a strain in which luminescence is independent of the QS system would be beneficial but no suitable construct is currently available.

3. Conclusion

A series of nine flavonoids, including four new ones were isolated from the leaves of *P. delineatum*. Two compounds from this series, **3** and **7**, displayed a potent QS inhibitory activity in *V. harveyi* without inhibition of bacterial growth up to 500 μM. Experiments with *V. harveyi* mutant strains suggest a molecular target downstream LuxO for these compounds. In addition, both flavonoids exhibited a strong inhibitory effect on biofilm formation in *V. harveyi*. These results emphasize the potential of naturally occurring plant secondary metabolites, in particular flavonoids, to interfere with bacterial processes. Further investigations will be conducted to deepen our understanding of the mechanism of action of this series of flavonoids.

4. Experimental

4.1. General experimental procedures

Optical rotations were measured on a Perkin Elmer 241 automatic polarimeter in $CHCl_3$ at 25 °C and the $[\alpha]_D$ values are given in 10^{-1} deg cm^2/g. UV spectra were obtained in absolute EtOH on a JASCO V-560 spectrophotometer. IR (film) spectra were measured on a Bruker IFS 55 spectrophotometer. ^{1}H and ^{13}C (400 and 100 MHz, respectively) NMR spectra were recorded in $(CD_3)_2CO$ on a Bruker Avance 400 spectrometer; the chemical shifts are given in δ (ppm) with TMS as internal reference and coupling constants in Hz. DEPT, COSY, ROESY (spin lock field 2500 Hz), HSQC and HMBC (optimized for J = 7.7 Hz) experiments were conducted on a Bruker Avance 500 spectrometer at 500 MHz with the pulse sequences given by Bruker. EIMS and HREIMS were collected with a Micromass Autospec spectrometer. Silica gel 60 (particle size 15–40 and 63–200 μm, Macherey–Nagel) and Sephadex LH-20 (Pharmacia Biotech) were used for column chromatography, silica gel 60 F254 (Macherey–Nagel) were used for analytical or preparative TLC, and nanosilica gel 60 F254 (Macherey–Nagel) for high-performance TLC (HPTLC). Centrifugal preparative TLC (CPTLC) was performed using a Chromatotron (Harrison Research Inc. model 7924T) on 1, 2, or 4 mm silica gel PF254 disks with flow rate 2–4 ml/min. The spots were visualized by UV light and heating silica gel plates sprayed with H_2O–H_2SO_4–AcH (1:4:20). All solvents used were analytical grade from Panreac.

4.2. Plant material

Leaves of *P. delineatum* were collected in Iquitos, Maynas Province, Department of Loreto, Perú in November 2009. A voucher specimen (10484) was identified by botanist Juan Ruiz Macedo and was deposited in the Amazonense Herbarium of the Universidad Nacional de la Amazonia Peruana, Iquitos, Peru.

4.3. Extraction and isolation

The air-dried leaves of *P. delineatum* (252.2 g) were ground and extracted with EtOH (4 l) in a Soxhlet apparatus. Evaporation of the solvent under reduced pressure provided 57.3 g (22.7%) of crude extract, which was successively partitioned into CH_2Cl_2/H_2O (1:1, v/v) solution. Removal of the CH_2Cl_2 from the organic-soluble extract under reduced pressure yielded 30 g (11.9%) of residue. The CH_2Cl_2 residue was chromatographed on a silica gel column, using mixtures of hexanes/EtOAc of increasing polarity (10:0–0:10) as eluent to afford 19 fractions which were combined based on their TLC profile in A–J junctions. Preliminary ^{1}H NMR analysis revealed that fractions C (hexanes/EtOAc, 8:2), H (hexanes/EtOAc, 3:7) and J (EtOAc) were rich in flavonoids, and were further investigated. Fraction C (2.2 g) was chromatographed on Sephadex LH-20 (hexanes/$CHCl_3$/MeOH, 2:1:1) to afford fractions C1–C5. Fraction C3 (328.8 mg) was chromatographed by CPTLC using mixtures of hexanes/Et_2O of increasing polarity (8:2–1:1) as eluent to afford eleven fractions (C3A–C3K). Subfractions C3E (16.4 mg) and C3H (17.7 mg) were further purified by HPTLC (hexanes/EtOAc, 8:2 and hexanes/CH_2Cl_2, 8:2, respectively) to give compound **9** (9.4 mg), and compounds **8** (3.6 mg) and **5** (8.3 mg), respectively. Fraction H (5.4 g) was chromatographed on Sephadex LH-20 ($CHCl_3$/MeOH, 1:1) to afford fractions H1–H9. Fraction H6 (304.8 mg) was chromatographed by CPTLC (CH_2Cl_2/acetone of increasing polarity, 10:0–1:1) to afford nine fractions (H6A–H6I). Subfraction H6F (18.2 mg) was further purified by HPTLC (hexanes/EtOAc, 3:2) to give compounds **1** (4.7 mg) and **6** (9.3 mg). Fraction H7 (593.0 mg) was chromatographed by CPTLC

(CH_2Cl_2–acetone, 10:0–1:1) to give fractions H7A–H7G. Subfraction H7F (23.1 mg) was further purified by HPTLC (hexanes/isopropanol, 4:1) to yield compounds **2** (15.3 mg) and **7** (3.8 mg). Fraction J (3.9 g) was chromatographed on Sephadex LH-20 ($CHCl_3$/MeOH, 1:1) to afford fractions J1–J5. Fraction J3 (628.8 mg) was chromatographed by CPTLC (CH_2Cl_2/acetone, 10:0–7:3) to afford fractions J3A–J3L. Subfractions J3F (16.4 mg) and J3H (21.2 mg) were further purified by HPTLC (CH_2Cl_2/acetone, 9:1 and hexanes/isopropanol, 8:2, respectively) to afford compounds **4** (11.4 mg) and **3** (10.4 mg), respectively.

4.4. 2′,4′-Dihydroxy-3,3′,6′-trimethoxychalcone (**1**)

Yellow amorphous solid; UV λ_{max} (MeOH) ($\log\varepsilon$) 211 (3.2), 345 (2.9) nm; IR ν_{max} (film) 3375, 2919, 2850, 1725, 1628, 1586, 1429, 1331, 1259, 1196, 1159, 1110, 1010, 977, 851, 786, 726 cm^{-1}; ^1H NMR [$(CD_3)_2CO$] δ 3.77 (3H, s, OCH_3-3′), 3.87 (3H, s, OCH_3-3), 3.97 (3H, s, OCH_3-6′), 9.22 (1H, s, OH-4′), 14.34 (1H, s, OH-2′), for other signals, see Table 1; ^{13}C NMR [$(CD_3)_2CO$] δ 55.6 (q, OCH_3-3), 56.5 (q, OCH_3-6′), 60.6 (q, OCH_3-3′), for other signals, see Table 1; EIMS *m/z* 330 [M^+] (81), 300 (25), 223 (14), 196 (100), 181 (13), 150 (20), 138 (4); HREIMS *m/z* 330.1104 [M^+] (calcd for $C_{18}H_{18}O_6$, 330.1103).

4.5. 2′,3′,5-Trihydroxy-4′,6′,3-trimethoxychalcone (**2**)

Yellow amorphous solid; UV λ_{max} (MeOH) ($\log\varepsilon$) 209 (4.6), 346 (3.9) nm; IR ν_{max} (film) 3417, 3010, 2944, 2851, 1733, 1635, 1596, 1565, 1458, 1432, 1319, 1288, 1233, 1214, 1118, 1084, 1063, 976, 899, 843, 806, 759, 683 cm^{-1}; ^1H NMR [$(CD_3)_2CO$] δ 3.82 (3H, s, OCH_3-5), 3.96 (3H, s, OCH_3-4′), 4.01 (3H, s, OCH_3-6′), 6.91 (1H, s, OH-3′), 8.62 (1H, br s, OH-3), 13.81 (1H, s, OH-2′), for other signals, see Table 1; ^{13}C NMR [$(CD_3)_2CO$] δ 55.6 (q, OCH_3-5), 56.5 (q, OCH_3-4′), 56.7 (q, OCH_3-6′), for other signals, see Table 1; EIMS *m/z* 346 [M^+] (55), 316 (42), 297 (33), 223 (12), 196 (100), 181 (18), 178 (13), 167 (10), 150 (31), 91 (7), 57 (8); HREIMS *m/z* 346.1053 [M^+] (calcd for $C_{18}H_{18}O_7$, 346.1037).

4.6. (−)-(2S)-7,5′-Dihydroxy-5,3′-dimethoxyflavanone (**3**)

Yellow amorphous solid; $[\alpha]_D^{20}$ −11.1 (*c* 0.26, MeOH); UV λ_{max} (MeOH) ($\log\varepsilon$) 203 (4.8), 226 (4.5), 284 (4.4) nm; IR ν_{max} (film) 3432, 2925, 2854, 1937, 1729, 1605, 1462, 1378, 1264, 1162, 1113, 1076, 884, 828, 756 cm^{-1}; ^1H NMR [$(CD_3)_2CO$] δ 3.77 (3H, s, OCH_3-5′), 3.79 (3H, s, OCH_3-5), 8.51 (1H, s, OH-3′), 9.41 (1H, s, OH-7), for other signals, see Table 1; ^{13}C NMR [$(CD_3)_2CO$] δ 55.6 (q, OCH_3-5′), 56.1 (q, OCH_3-5), for other signals, see Table 1; EIMS *m/z* 316 [M^+] (100), 299 (8), 193 (68), 167 (62), 150 (14), 138 (9); HREIMS *m/z* 316.0932 [M^+] (calcd for $C_{17}H_{16}O_6$, 316.0947).

4.7. (−)-(2S)-8-Hydroxy-5,7,3′-trimethoxyflavanone (**4**)

Yellow amorphous solid; $[\alpha]_D^{20}$ −12.1 (*c* 0.30, MeOH); UV λ_{max} (MeOH) ($\log\varepsilon$) 206 (5.6), 243 (5.1), 285 (5.2), 348 (3.8) nm; IR ν_{max} (film) 3388, 3006, 2924, 2848, 1725, 1666, 1613, 1588, 1512, 1494, 1462, 1438, 1417, 1370, 1346, 1265, 1210, 1155, 1111, 1046, 1013, 919, 856, 792, 755, 702 cm^{-1}; ^1H NMR [$(CD_3)_2CO$] δ (3H, s, OCH_3-5), 3.83 (3H, s, OCH_3-3′), 3.94 (3H, s, OCH_3-7), 7.22 (1H, s, OH-8), for other signals, see Table 1; ^{13}C NMR [$(CD_3)_2CO$] δ 55.6 (q, OCH_3-3′), 56.5 (2 × q, OCH_3-5, OCH_3-7), for other signals, see Table 1; EIMS *m/z* 330 [M^+] (62), 196 (100), 178 (8), 150 (21); HREIMS *m/z* 330.1111 [M^+] (calcd for $C_{18}H_{18}O_6$, 330.1103).

4.8. Quorum sensing assays

V. harveyi wild type strain BB120 and mutants BB170 (luxN::Tn5kan), BB886 (luxPQ::Tn5kan) and BB721 (luxO::Tn5lacZ) were acquired from ATCC. To evaluate the QS inhibitory activity of the flavonoids, a screening procedure was adapted from (Defoirdt et al., 2007, 2012), with slight modifications. Bacteria were cultured in Luria–Bertani medium containing 35 g/l sea salts (Sigma–Aldrich). Stock solutions of the test compounds in DMSO (40 mM) were serially diluted at 2× final test concentrations in white, clear-bottom 96-well microtiter plates (Costar 3610) containing 100 µl of culture medium. Bacterial inocula (100 µl) were prepared from 1:50 dilutions of overnight cultures, giving a starting cell density of 1–2 × 10^7 cfu ml^{-1}. The microtiter plates were covered with a clear sterile sealing film and incubated at 30 °C with agitation (150 rpm). Luminescence and OD_{600} were monitored every 15 min over 18 h with a multimode plate reader (Perkin-Elmer EnSpire) in order to correlate simultaneously any possible decrease in the luminescent phenotype with a growth-inhibitory effect.

4.8.1. Calculations and statistics

For the determination of the IC_{50} values for bioluminescence and growth, the area under each luminescence or growth curve, respectively, at each dose and for each reporter strain were calculated. Inhibitions were calculated with respect to the untreated control as follows:

$I = [(A_c - A_t)/A_c] * 100$, where I is the inhibition (%), A_c is the area under the control curve and A_t is the area under each treatment curve. These values were plotted against the corresponding $\log C$ values (C = concentration) and adjusted to a four-parameter nonlinear regression model with GraphPad Prism v.5 (GraphPad Software Inc., La Jolla, CA, USA). The relative luminescence values, designed as Relative Luminescence Units (RLU) were obtained by dividing the area under the luminescence curve by that under the growth curve for each dose, in order to normalize bioluminescence data with respect to bacterial growth. When indicated, statistical analysis (one-way ANOVA with Dunnett's multiple comparisons test) was performed with Sigmaplot 12 (Systat Software Inc., San José, CA, USA). The assumptions of independence, normality and homoscedasticity were verified prior to ANOVA calculations. The limit for statistical significance was established at $P = 0.05$.

4.8.2. Biofilm assays

Vibrio harveyi BB120 was incubated overnight and diluted to a cell density of 1 × 10^8 cfu ml^{-1}. For biofilm tests, Marine Broth (Panreac) was employed since biofilm formation is strongly promoted in this medium. One-hundred microliter of bacterial suspension were inoculated in each well of a microtiter plate (Nunc 167008) containing serial dilutions (100 µl) of the test compounds. The plates were incubated at 30 °C for 24 h. Then, OD600 readings were taken to quantify bacterial growth. Plates were emptied, thoroughly rinsed with saline solution (×3), and finally stained with 0.2% crystal violet for 15 min. Plates were rinsed to remove the excess dye and dried at room temperature. Bound crystal violet was re-solubilized by addition of 200 µl EtOH and OD readings were taken at 590 nm.

Acknowledgements

We are indebted to the Spanish Ministry of Economy and Competitiveness (MINECO) SAF2011-28883-C03-01 and CTQ2014-55888-C03-01-R; EU, FP7-REGPOT-2012-CT2012-316137-IMBRAIN; and Campus de Excelencia Internacional CEI10/00018 projects for financial support. A.J.M.-R. thanks

PLOCAN for a 2+2 contract. The authors are grateful to Dr. Tom Defoirdt (University of Ghent) for his valuable advice in the experimental set-up with *Vibrio harveyi*.

Appendix A. Supplementary data

Supplementary data associated with this article can be found, in the online version, at http://dx.doi.org/10.1016/j.phytochem.2015.06.006.

References

Andersen, O.M., Markham, K.R., 2006. Flavonoids, Chemistry, Biochemistry and Applications. Taylor and Francis, Boca Ratón, Florida.

Anetzberger, C., Schell, U., Jung, K., 2012. Single cell analysis of *Vibrio harveyi* uncovers functional heterogeneity in response to quorum sensing signals. BMC Microbiol. 12, 209.

Aponte, J.C., Castillo, D., Estevez, Y., Gonzalez, G., Arevalo, J., Hammond, Gerald B., Sauvain, M., 2010. *In vitro* and *in vivo* anti-leishmania activity of polysubstituted synthetic chalcones. Bioorg. Med. Chem. Lett. 20, 100–103.

Bjarnsholt, T., Ciofu, O., Molin, S., Givskov, M., Hoiby, N., 2013. Applying insights from biofilm biology to drug development – can a new approach be developed? Nat. Rev. Drug Discov. 12, 791–808.

Boumendjel, A., Boccard, J., Carrupt, P.-A., Nicolle, E., Blanc, M., Geze, A., Choisnard, L., Wouessidjewe, D., Matera, E.-L., Dumontet, C., 2008. Antimitotic and antiproliferative activities of chalcones: forward structure–activity relationship. J. Med. Chem. 51, 2307–2310.

Chantrapromma, K., Rat-A-pa, Y., Karalai, C., Lojanapiwatana, V., Seechammanturakit, V., 2000. A chalcone and a dihydrochalcone from *Uvaria dulcis*. Phytochemistry 53, 511–513.

Cushnie, T.P.T., Lamb, A.J., 2011. Recent advances in understanding the antibacterial properties of flavonoids. Int. J. Antimicrob. Agents 38, 99–107.

Defoirdt, T., Benneche, T., Brackman, G., Coenye, T., Sorgeloos, P., Scheie, A.A., 2012. A quorum sensing-disrupting brominated thiophenone with a promising therapeutic potential to treat luminescent *Vibriosis*. PLoS One 7, e41788.

Defoirdt, T., Boon, N., Sorgeloos, P., Verstraete, W., Bossier, P., 2008. Quorum sensing and quorum quenching in *Vibrio harveyi*: lessons learned from *in vivo* work. ISME J. 2, 19–26.

Defoirdt, T., Boon, N., Bossier, P., 2010. Can bacteria evolve resistance to quorum sensing disruption? PLoS Pathog. 6, e1000989.

Defoirdt, T., Brackman, G., Coenye, T., 2013. Quorum sensing inhibitors: how strong is the evidence? Trends Microbiol. 21, 619–624.

Defoirdt, T., Miyamoto, C.M., Wood, T.K., Meighen, E.A., Sorgeloos, P., Verstraete, W., Bossier, P., 2007. The natural furanone (5*Z*)-4-bromo-5-(bromomethylene)-3-butyl-2(5H)-furanone disrupts quorum sensing-regulated gene expression in *Vibrio harveyi* by decreasing the DNA-binding activity of the transcriptional regulator protein luxR. Environ. Microbiol. 9, 2486–2495.

Dobretsov, S., Dahms, H.-U., YiLi, H., Wahl, M., Qian, P.-Y., 2007. The effect of quorum-sensing blockers on the formation of marine microbial communities and larval attachment. FEMS Microbiol. Ecol. 60, 177–188.

Fu, X., Sevenet, T., Remy, F., Pais, M., Hadi, A., Hamid, A., Zeng, L.M., 1993. Flavanone and chalcone derivatives from *Cryptocarya kurzii*. J. Nat. Prod. 56, 1153–1163.

García-Contreras, R., Maeda, T., Wood, T.K., 2013. Resistance to quorum-quenching compounds. Appl. Environ. Microbiol. 79, 6840–6846.

Givskov, M., de Nys, R., Manefield, M., Gram, L., Maximilien, R., Eberl, L., Molin, S., Steinberg, P.D., Kjelleberg, S., 1996. Eukaryotic interference with homoserine lactone-mediated prokaryotic signaling. J. Bacteriol. 178, 6618–6622.

Harborne, J.B., Mabry, T.J., 1975. The Flavonoids. Chapman and Hall, London.

Henke, J.M., Bassler, B.L., 2004. Three parallel quorum-sensing systems regulate gene expression in *Vibrio harveyi*. J. Bacteriol. 186, 6902–6914.

Joint, I., Tait, K., Wheeler, G., 2007. Cross-kingdom signalling: exploitation of bacterial quorum sensing molecules by the green seaweed *Ulva*. Philos. Trans. R. Soc. Lond. B Biol. Sci. 362, 1223–1233.

Kalia, V.C., 2013. Quorum sensing vs quorum quenching: a battle with no end insight. Biotechnol. Adv. 31, 224–245.

Kuroyanagi, M., Noro, T., Fukushima, S., Aiyama, R., Ikuta, A., Itokawa, H., Morita, M., 1983. Studies on the constituents of the seeds of *Alpinia katsumadai* Hayata. Chem. Pharm. Bull. 31, 1544–1550.

Martín-Rodríguez, A.J., Babarro, J.M., Lahoz, F., Sansón, M., Martín, V.S., Norte, M., Fernández, J.J., 2015. From broad-spectrum biocides to quorum sensing disruptors and mussel repellents: antifouling profile of alkyl triphenylphosphonium salts. PLoS One 10, e0123652.

Mielich-Suss, B., López, D., 2015. Molecular mechanisms involved in *Bacillus subtilis* biofilm formation. Environ. Microbiol. 17, 555–565.

Miller, M.B., Bassler, B.L., 2001. Quorum sensing in bacteria. Annu. Rev. Micriobiol. 55, 165–169.

Nackerdien, Z.E., Keynan, A., Bassler, B.L., Lederberg, J., Thaler, D.S., 2008. Quorum sensing influences *Vibrio harveyi* growth rates in a manner not fully accounted for by the marker effect of bioluminescence. PLoS One 3, e1671.

Nazzaro, F., Fratianni, F., Coppola, R., 2013. Quorum sensing and phytochemicals. Int. J. Mol. Sci. 14, 12607–12619.

Pompeani, A.J., Irgon, J.J., Berger, M.F., Bulyk, M.L., Wingreen, N.S., Bassler, B.L., 2008. The *Vibrio harveyi* master quorum-sensing regulator, LuxR, a TetR-type protein is both an activator and a repressor: DNA recognition and binding specificity at target promoters. Mol. Microbiol. 70, 76–88.

Rutherford, S.T., Bassler, B.L., 2012. Bacterial quorum sensing: its role in virulence and possibilities for its control. Cold Spring Harb. Perspect. Med. 2, a012427.

Tan, L., Zhang, X.-F., Yan, B.-Z., Shi, H.-M., Du, L.-B., Zhang, Y.-Z., Wang, L.-F., Tang, Y.-L., Liu, Y., 2007. A novel flavonoid from *Lespedeza virgata* (Thunb.) DC.: structural elucidation and antioxidative activity. Bioorg. Med. Chem. Lett. 17, 6311–6315.

Twigg, M.S., Tait, K., Williams, P., Atkinson, S., Cámara, M., 2014. Interference with the germination and growth of Ulva zoospores by quorum sensing molecules produced by Ulva-associated epiphytic bacteria. Environ. Microbiol. 16, 445–453.

Vandeputte, O.M., Kiendrebeogo, M., Rajaonson, S., Diallo, B., Mol, A., El Jaziri, M., Baucher, M., 2010. Identification of catechin as one of the flavonoids from *Combretum albiflorum* bark extract that reduces the production of quorum-sensing-controlled virulence factors in *Pseudomonas aeruginosa* PAO1. Appl. Environ. Microbiol. 76, 243–253.

Vandeputte, O.M., Kiendrebeogo, M., Rasamiravaka, T., Stévigny, C., Duez, P., Rajaonson, S., Diallo, B., Mol, A., Baucher, M., El Jaziri, M., 2011. The flavanone naringenin reduces the production of quorum sensing-controlled virulence factors in *Pseudomonas aeruginosa* PAO1. Microbiology 157, 2120–2132.

Vikram, A., Jayaprakasha, G.K., Jesudhasan, P.R., Pillai, S.D., Patil, B.S., 2010. Suppression of bacterial cell–cell signaling, biofilm formation and type III secretion system by citrus flavonoids. J. Appl. Microbiol. 109, 515–527.

Vogel, S., Barbic, M., Jürgenliemk, G., Heilmann, J., 2010. Synthesis, cytotoxicity, anti-oxidative and anti-inflammatory activity of chalcones and influence of A-ring modifications on the pharmacological effect. Eur. J. Med. Chem. 45, 2206–2213.

Waters, C.M., Bassler, B.L., 2005. Quorum sensing: cell-to-cell communication in bacteria. Annu. Rev. Cell Dev. Biol. 21, 319–346.

Waters, C.M., Bassler, B.L., 2006. The *Vibrio harveyi* quorum-sensing system uses shared regulatory components to discriminate between multiple autoinducers. Genes Dev. 20, 2754–2767.

Yebra, D.M., Kiil, S., Dam-Johansen, K., 2004. Antifouling technology-past, present and future steps towards efficient and environmentally friendly antifouling coatings. Prog. Org. Coat. 50, 75–104.